Colloids and Surfaces A: Physicochem. Eng. Aspects 379 (2011) 143–150

Contents lists available at ScienceDirect

Colloids and Surfaces A: Physicochemical and Engineering Aspects

journal homepage: www.elsevier.com/locate/colsurfa

Reduction of iron oxides by *Klebsiella pneumoniae* L17: Kinetics and surface properties

Tong-xu Liu, Xiao-min Li, Fang-bai Li*, Wei Zhang, Man-jia Chen, Shun-gui Zhou

Guangdong Key Laboratory of Agricultural Environment Pollution Integrated Control, Guangdong Institute of Eco-Environmental and Soil Sciences, Guangzhou, China

ARTICLE INFO

Article history:
Received 28 June 2010
Received in revised form 16 October 2010
Accepted 18 November 2010
Available online 8 December 2010

Keywords:
Klebsiella pneumoniae L17
Reduction
Iron oxides
Secondary minerals
AQDS

ABSTRACT

The kinetics of the reduction dissolution of iron oxides was studied by using *Klebsiella pneumoniae* L17 in a pH 7.0 bicarbonate buffer. The microbial reduction of various iron oxides was measured in the absence and presence of AQDS (9,10-anthraquinone-2,6-disulfonic acid), and the results of their rates vs. the surface areas of iron oxides suggested that the iron oxide reduction rate by L17 was obviously affected by the surface area but did not completely depend on it especially for hydrous ferric oxide. Increasing the crystalline degree of hematite decreased the rate of iron reduction, indicating that a higher crystalline degree inhibited microbial iron reduction. Increasing the AQDS concentration significantly increased the rate of HFO reduction, which suggested that the addition of AQDS significantly accelerated the microbial reduction of crystalline Fe(III) oxides. From the increased production of AH_2DS (2,6-anthrahydroquinone disulfonate) and cell numbers, it can be concluded that the enhancement may be because of the growth in cells and abiotic Fe(III) reduction by AH_2DS. X-ray diffraction, Fourier transform infrared spectra and scanning electron microscopy all indicated that secondary minerals (e.g., vivianite ($Fe_3(PO_4)_2$) and siderite ($FeCO_3$)) were the biogenic Fe(II) solids formed upon the bioreduction of iron oxides.

1. Introduction

Iron is the most abundant transition metal element on Earth, and iron-bearing minerals are ubiquitous reactive constituents of soils, sediments and aquifers. The cycle of iron has a profound effect on the geochemistry of other elements and contaminants in groundwater and sedimentary environments, especially the reduction of iron(III). The reduction of even a minor amount of iron in iron-bearing minerals could significantly influence the inorganic and organic geochemistry of such environments [1,2]. First, iron-bearing minerals exhibit large surface areas that bind trace metals (e.g., arsenic and zinc), nutrients (e.g., phosphate, trace metals) and organic molecules (e.g., nitro- and chlorinated organic compounds). Second, the ferrous iron-containing minerals produced during the reductive dissolution can provide a reactive Fe(II) surface capable of participating in secondary redox or mineral-forming reactions [3,4]. The transformation of reducible substrates may strongly depend on the biogeochemistry of iron species under anaerobic conditions. Hence, an understanding of the biogeochemical redox processes of iron is important for predicting contamination transformations and can provide new opportunities for engineered remediation strategies.

Iron reduction in anoxic conditions is dominated by iron-reducing microorganisms. Dissimilatory iron-reducing bacteria (DIRB) are a group of microorganisms that can oxidize organic matter and reduce Fe(III) to Fe(II) under anoxic conditions [5]. They include both facultative and obligate anaerobes and can be classified as fermentative, photosynthetic, organic acid-oxidizing and hydrogen-oxidizing bacteria [6]. *Geobacter* and *Shewanella* [7] are representative species of DIRB and have been extensively investigated with respect to their ability to reduce Fe(III) [8]. However, *Geobacter* species are obligate anaerobes found in anaerobic sediment environments, whereas *Shewanella* species are facultative anaerobes, which are not the dominant DIRB in anaerobic environments according to many molecular biological studies [7]. So far, seldom research has been conducted to investigate the iron oxide reduction by other DIRB commonly found in the aerobic–anaerobic environments.

Biotic iron reduction is complicated in the natural environment; therefore, it is necessary to clearly illustrate the main factors of influence. First is the crystalline structure and degree of iron-bearing minerals. Iron(III) oxides are among the most abundant forms of Fe(III) in near-surface aquatic and terrestrial systems, which are relatively insoluble at circumneutral pH. Amorphous Fe(III) oxides (e.g., ferrihydrite) are partly reducible and presumably the dominant component of reducible Fe(III) [9],

* Corresponding author at: Guangdong Institute of Eco-Environmental and Soil Sciences, No. 808, Tianyuan Road, Tianhe District, Guangzhou 510650, China. Tel.: +86 20 87024721; fax: +86 20 87024123.
E-mail address: cefbli@soil.gd.cn (F.-b. Li).

0927-7757/$ – see front matter © 2010 Elsevier B.V. All rights reserved.
doi:10.1016/j.colsurfa.2010.11.061

whereas crystalline Fe(III) oxides (e.g., magnetite and goethite) have much less reducibility [10]. Bonneville et al. [11] demonstrated that the abiotic rate of reductive dissolution correlated with the solubility of iron oxides. Roden and Zachara [12] indicated that the initial rate and long-term extent of iron(III) oxide reduction were linearly correlated with oxide surface area. However, not only the surface areas but also the crystalline degrees of iron oxides are related to their crystal structures, which might tightly correlate to the dissimilatory iron reduction.

Second is the natural electron shuttle, such as the humic acid, fulvic acid and other quinone-containing compounds. Humic substances are redox-active and can be reduced by microorganisms under anaerobic conditions. They can stimulate the microbial reduction of poorly soluble Fe(III) minerals by acting as electron shuttles between cell and mineral [13–15]. O'Loughlin [16] investigated the effects of a series of natural and synthetic organic electron shuttles on the bioreduction of lepidocrocite by *Shewanella putrefaciens* CN32 and found that the rate of Fe(II) production correlated with the reduction potentials of the electron shuttles. However, Wolf et al. [17] found that the redox potentials of the most active quinones fall in a narrow range of −137 to −225 mV vs. NHE (normal hydrogen electrode) at pH 7.0, of which AQDS (9,10-anthraquinone-2,6-disulfonic acid) was the most effective. It has also been suggested that the rate of microbial iron reduction mediated by electron shuttles is mainly controlled by the redox potential of the shuttle compound rather than by the proportion of dissolved vs. adsorbed compounds. In addition, humic substances further influence the formation (biomineralization) of Fe minerals, both through the complexation and solubilization of metal ions and by sorption to the mineral surface, generally causing less crystalline minerals to form [18].

Third is the secondary mineral. Readsorption can cause structural changes in the host Fe hydroxide minerals, potentially leading to the formation of such Fe(II)-bearing minerals as green rust and magnetite. The knowledge of the conditions under which Fe oxyhydroxides transform, and the particular secondary phases they transform to, in the subsurface is important for understanding their occurrences and for predicting the mobility of aqueous environmental contaminants that are influenced by these phases [1]. The reduction of Fe(III) minerals produces soluble Fe(II) as well as a wide range of secondary minerals, including Fe(II) minerals (e.g., vivianite ($Fe_3(PO_4)_2$) and siderite ($FeCO_3$)), Fe(III) minerals (e.g., goethite) and mixed Fe(II)/Fe(III) minerals (e.g., magnetite (Fe_3O_4) and green rust (Fe(II)/Fe(III)-layered double hydroxides)). Dissolved, adsorbed and solid state Fe(II) can act as powerful reductants in a variety of abiotic redox processes [19].

A fermentative facultative anaerobe, *Klebsiella pneumoniae* L17, has been found to be capable of Fe(III) reduction in anaerobic environments [20]. In this study, the aim was to investigate the effects of AQDS, crystalline structure and crystalline degree on iron(III) reduction processes by *K. pneumoniae* L17 as well as changes in the iron minerals before and after iron reduction. The obtained results of this study are anticipated to be valuable and important for understanding and adjusting the iron reduction process, which is important for assessing the biogeochemical process of iron in iron-rich soils.

2. Materials and methods

2.1. Materials

K. pneumoniae strain L17, a fermentative facultative anaerobe, was isolated previously from the subterranean forest sediment in Zhaoqing, China [20]. AQDS (97.0%) was purchased from Fluka without further purification. Other chemicals, being of analytical grade, were obtained from Shanghai Chemical Co., China.

2.2. Fe(III) oxide preparation and characterization

According to McCormick and Adriaens [21], hydrous ferric oxide (HFO) was prepared by slowly neutralizing 0.4 mM solution of $FeCl_3{\cdot}6H_2O$ with 1 mM NaOH in a high-density polyethylene container. Thick red slurry of HFO formed as pH 7.0 was approached, and the slurry was allowed to ripen for 2–6 h, with a slight decrease in pH (usually <1 pH unit). The slurry was adjusted back to pH 7.0 and centrifuged at 3600 × *g* for 20 min at 4 °C. After decanting the supernatant, the solid was resuspended and washed with Milli-Q water and centrifuged again. This procedure was repeated seven times to reduce the chloride content to less than 1 mM. Goethite (α-FeOOH) was prepared according to the procedures of Schwertmann and Cornell [22]. 0.05 mol of hydrated ferric nitrate ($Fe(NO_3)_3{\cdot}9H_2O$) was dissolved in 0.45 mol potassium hydroxide and then diluted to 1.0 L. The solution was refluxed at 70 °C for 60 h. Then, the hydrosol was washed until neutral with Milli-Q water and dried at 65 °C for 48 h. Lepidocrocite (γ-FeOOH) was synthesized by mixing $FeCl_2{\cdot}4H_2O$, $(CH_2)_6N_4$ and $NaNO_2$ in Milli-Q water, and hematite (α-Fe_2O_3) was formed by sintering γ-FeOOH powder at 300, 400, 500, 600, 700 and 800 °C, respectively for 2 h at 2 °C min^{-1} temperature increase rate [23]. All iron oxides were ground to pass through a 100 mesh sieve, except HFO.

2.3. Fe(III) reduction experiments

The medium was used as before [20], which contained the following components (per liter of deionized H_2O): $NaHCO_3$, 2.5 g; NH_4Cl, 0.25 g; $NaH_2PO_4{\cdot}2H_2O$, 0.68 g; KCl, 0.10 g; the mineral solution, 10 mL; the vitamin solution, 10 mL. Harvested cells of *K. pneumoniae* L17 were used for the Fe(III) reduction experiments. Cells were grown in nutrient broth under aerobic conditions on a rotary shaker at 180 rpm at 30 °C, and harvested by centrifugation at 6900 × *g* for 10 min at 4 °C when it approached the exponential phase. The pellets were washed three times and resuspended in sterile fresh basal medium. The initial concentrations of cells in all Fe(III) reduction experiments were 1.5×10^8 cells mL^{-1}.

Glycerol (10 mM) or glucose (5 mM) was used as the electron donor and 50 mM of HFO, α-FeOOH, γ-FeOOH or α-Fe_2O_3 was added as electron acceptors into the medium to investigate the rate and extent of Fe(III) oxide reduction by *K. pneumoniae* L17. AQDS was added at final concentrations of 10, 100 and 1000 μM to estimate its effect on microbial Fe(III) reduction. All experiments were conducted in duplicate using standard anaerobic techniques. All anaerobic media were boiled and cooled under a constant stream of 80% N_2–20% CO_2, dispensed into aluminum-sealed culture bottles under the same gas phase, capped with butyl rubber stoppers and sterilized by autoclaving (121 °C, 20 min). Besides the sterile media, inoculation and sampling were conducted by using sterile syringes and needles. All vials were incubated in a Bactron Anaerobic/Environmental Chamber II (Shellab, Sheldon Manufacturing Inc., Cornelius, OR, USA) at 30 °C in the dark.

2.4. Analytical methods

The total concentration of Fe(II), including dissolved and sorbed Fe(II), was determined by extracting Fe(II) from the samples using 0.5 mol L^{-1} HCl for 1.5 h [5] and assaying the extract using 1,10-phenanthroline colorimetric assay [24]. Goethite, lepidocrocite and hematite were well crystallized by X-ray diffraction (XRD). To determine the crystal phase composition of the iron oxides before and after reduction, XRD measurements were taken at room temperature using a Rigaku D/MAX-IIIA diffractometer with Cu Kα radiation. An accelerating voltage of 35 kV and emission current

of 30 mA were used. The total surface area was measured by the Brunauer–Emmett–Teller (BET) method using a Coulter SA-3100, in which an N_2 adsorption at 77 K was applied and a Carlo Erba sorptometer was used. Fourier transform infrared spectra (FTIR) measurements were taken using a FTIR spectrometer (Perkin-Elmer, model Vector 33, Bruker Co.) at room temperature. Four iron oxides before and after reduction were also examined by scanning electron microscopy (SEM) with a secondary electron detector (Leica, Stereoscan 440). Energy dispersion X-ray (EDX) analysis was also obtained through the SEM equipped with a link analyzer (Oxford, ISIS-300) to determine the amount of elements on the surfaces of oxides.

3. Results and discussion

3.1. Various iron oxide reductions by L17 with/without AQDS

Fig. 1a shows that Fe(II) production increased as time elapsed. Fe(II) concentrations were increased to 0.419 mM, 0.630 mM, 0.342 mM and 0.090 mM after 25 days for HFO, α-FeOOH, γ-FeOOH and α-Fe_2O_3, respectively, so the order was ranked as α-FeOOH > HFO > γ-FeOOH > α-Fe_2O_3. Uninoculated controls without L17 were conducted and the results (not shown) showed that no significant amount of Fe(II) was produced for all the oxides, indicating that the reduction of Fe(III) to Fe(II) is a biological transformation rather than a chemical reaction. When AQDS was added, Fe(II) production increased significantly in all inoculated vials (Fig. 1b). Fe(II) concentrations were increased to 4.59 mM, 4.80 mM, 2.38 mM and 0.45 mM after 25 days for HFO, α-FeOOH, γ-FeOOH and α-Fe_2O_3, respectively, so the order was ranked as α-FeOOH > HFO > γ-FeOOH > α-Fe_2O_3. In comparison to the system of L17 alone without AQDS, the Fe(II) reduction amount was significantly enhanced in the presence of AQDS, but the orders of them were not exactly the same. To clearly illustrate the Fe(II) production rates in both systems, the reduction rates were calculated using a zero-order kinetics model over the first 15 days of reduction. The results of Fe(II) production rates with L17 alone were 0.0100 mM day^{-1} (R = 0.996), 0.0207 mM day^{-1} (R = 0.961), 0.0187 mM day^{-1} (R = 0.996) and 0.0058 mM day^{-1} (R = 0.997) for HFO, α-FeOOH, γ-FeOOH and α-Fe_2O_3, respectively, whereas those with both L17 and AQDS were 0.102 mM day^{-1} (R = 0.900), 0.0753 mM day^{-1} (R = 0.976), 0.100 mM day^{-1} (R = 0.954) and 0.0303 mM day^{-1} (R = 0.921), which were 10.2, 3.6, 5.4 and 5.2 times greater than the results without AQDS. Furthermore, the surface areas were tested using the BET method and ranked as HFO (254.7 $m^2\ g^{-1}$) > α-FeOOH (120.9 $m^2\ g^{-1}$) > γ-FeOOH (115.4 $m^2\ g^{-1}$) > α-Fe_2O_3 (29.4 $m^2\ g^{-1}$). Hence, the Fe(II) production rates by L17 with/without AQDS vs. the surface areas were plotted in Fig. 1c, which showed that α-Fe_2O_3—with the lowest surface area—showed the lowest Fe(II) production rate, whereas α-FeOOH and γ-FeOOH—with adjacent surface areas—had the similar Fe(II) production rates in the system both with and without AQDS. It was noted that the HFO with the highest surface area showed a very low Fe(II) production rate with L17 alone, but was sharply accelerated in the presence of AQDS. Based on the above results, it can be concluded that the iron oxide reduction rate by L17 was obviously affected by the surface area but does not completely depend on it.

HFO, α-FeOOH, γ-FeOOH and α-Fe_2O_3, representing different types of iron oxides, are abundant in soil [25]. The properties of Fe(III) oxide, such as crystallinity, surface area, solubility and phase identity, have been demonstrated as major factors controlling the microbial reduction of Fe(III) oxide [11,26,27]. Roden and Zachara [12] found that the rate and extent of microbial Fe(III) oxide reduction increased linearly with surface area, regardless of the degree

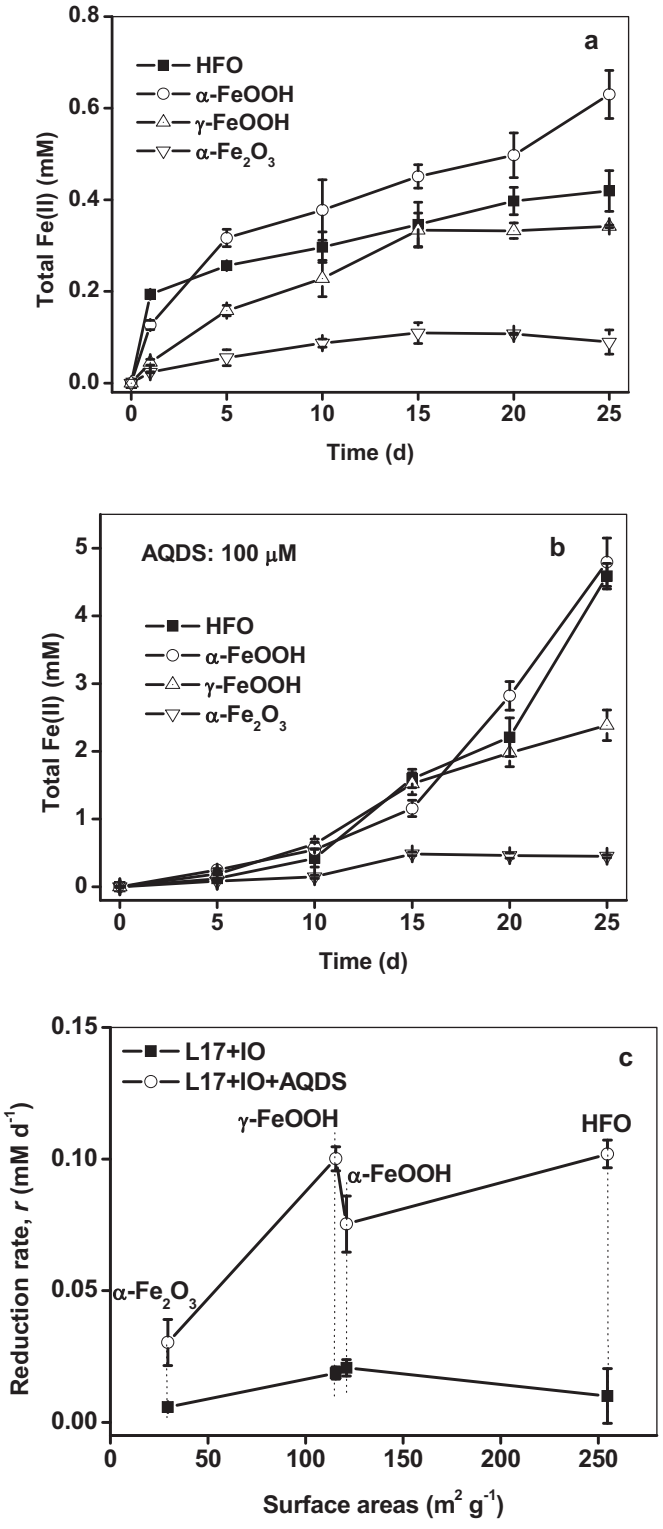

Fig. 1. Total Fe(II) production during various iron oxide reductions by L17 (a) without AQDS and (b) with AQDS. (c) The comparison of zero-order rate constants (k, mM day^{-1}) calculated from (a) and (b) over the first 15 days of reduction. The initial concentrations of other substrates were all iron oxides (50 mM), L17 (1.5×10^8 cells mL^{-1}) and AQDS (100 μM). Data are means ± SD (n = 3).

of Fe(III) oxide crystallinity or structural form. However, the results in this study suggest that the surface areas indeed correlate to the rate of Fe(III) oxide reduction by L17, but some other factors may also influence the microbial reduction rates and extents. It has been indicated that the abiotic rate of reductive dissolu-

tion correlates with the solubility of the iron oxides [11], which may be mainly attributed to the structure and crystallinity of iron oxides. In addition, the presence of AQDS was expected to accelerate the limited rate of Fe(III) oxide reduction, because AQDS can serve to shuttle electrons from DIRB to Fe(III) oxides in anaerobic soils and sediments [13–15]. For the HFO in this study, the addition of AQDS can obviously accelerate the iron reduction rate, but enhancements in the other three types of iron oxides were different. To clearly illustrate the role of crystalline degree and AQDS concentration on Fe(III) reduction by L17, a series of experiments were conducted and the reason was further investigated in detail as follows.

3.2. Effect of α-Fe_2O_3 crystalline degree on Fe(II) production by L17

To investigate the crystalline degree of iron oxides on microbial iron reduction, a series of hematite (α-Fe_2O_3) were synthesized at 300 °C, 400 °C, 500 °C, 600 °C, 700 °C and 800 °C, and named as Hem-300, Hem-400, Hem-500, Hem-600, Hem-700 and Hem-800, respectively. The XRD patterns are shown in Fig. 2a. From the results, it can be seen that a classical hematite phase was formed when the temperature increased from 300 to 800 °C, and also the diffraction peaks increased gradually with increasing temperature. The effect of crystalline degree on microbial iron oxide reduction was tested using L17 and hematite synthesized at different calcinated temperatures. The results in Fig. 2b show that the Fe(II) productions were 0.225 mM, 0.089 mM, 0.065 mM, 0.042 mM, 0.036 mM and 0.031 mM after 14 days for α-Fe_2O_3 synthesized from 300 to 800 °C, respectively, showing that the reduction amounts of iron oxides gradually decreased as temperature increased. The calculated Fe(II) production rates and the peaks at $2\theta = 33.2°$ of XRD patterns in Fig. 2a were both plotted vs. temperatures (Fig. 2c). The results show that as temperature increases from 300 to 800 °C, the peaks at $2\theta = 33.2°$ were 685, 1355, 1791, 3031, 4493 and 5371, whereas the Fe(II) production rates were 0.0156 mM day^{-1} ($R = 0.960$), 0.00593 mM day^{-1} ($R = 0.939$), 0.00437 mM day^{-1} ($R = 0.957$), 0.00322 mM day^{-1} ($R = 0.988$), 0.00279 mM day^{-1} ($R = 0.979$) and 0.00222 mM day^{-1} ($R = 0.918$), respectively. This result clearly confirms that a higher crystalline degree is negative for microbial iron reduction by L17.

3.3. Effect of AQDS on HFO reduction by L17

The results in Fig. 1a suggest that microbial iron reduction by L17 can be clearly accelerated with AQDS addition, but the acceleration extent for different types of iron oxides are different. To further illustrate the influence of AQDS in detail, different concentrations of AQDS were added into the reaction system of L17 and HFO, with the results shown in Fig. 3a. It can be seen that the HFO reduction rate by L17 increased significantly as the AQDS concentrations increased. After 150 days of anaerobic reaction, Fe(II) production was more than 11 mM, 17 mM and 19 mM for 10 μM, 100 μM and 1000 μM of AQDS, respectively, which were all much more than that (5 mM) of the control without AQDS. Also, the Fe(II) production rates were calculated and plotted vs. AQDS concentrations (Fig. 3b). It can be seen that the Fe(II) production rates were 0.791 mM day^{-1} ($R = 0.877$), 2.25 mM day^{-1} ($R = 0.9326$), 3.48 mM day^{-1} ($R = 0.971$) and 4.39 mM day^{-1} ($R = 0.871$) for the AQDS concentrations of 0 μM, 10 μM, 100 μM and 1000 μM, respectively.

AQDS has been indicated to be the most effective electron transfer mediator among a series of natural and synthetic organic electron shuttles for microbial iron reduction [16,17]. The electron shuttling of electron transfer mediators permits DIRB to indirectly reduce Fe(III) oxides faster than Fe(III) is reduced in the absence of electron transfer mediators [17]. Furthermore, anaerobic respiration with AQDS as the terminal electron acceptor can yield energy to support cell growth by some bacteria [28]. In this study, the production of AH_2DS (2,6-anthrahydroquinone disulfonate) and an increase in cell numbers was observed when AQDS was added. This enhancement may be attributed to the growth in cells and abiotic Fe(III) reduction by AH_2DS, which was formed from the reduction of AQDS by L17. This suggests that Fe(III) oxide reduction by L17 may be favored in the natural environment where humic substances are present.

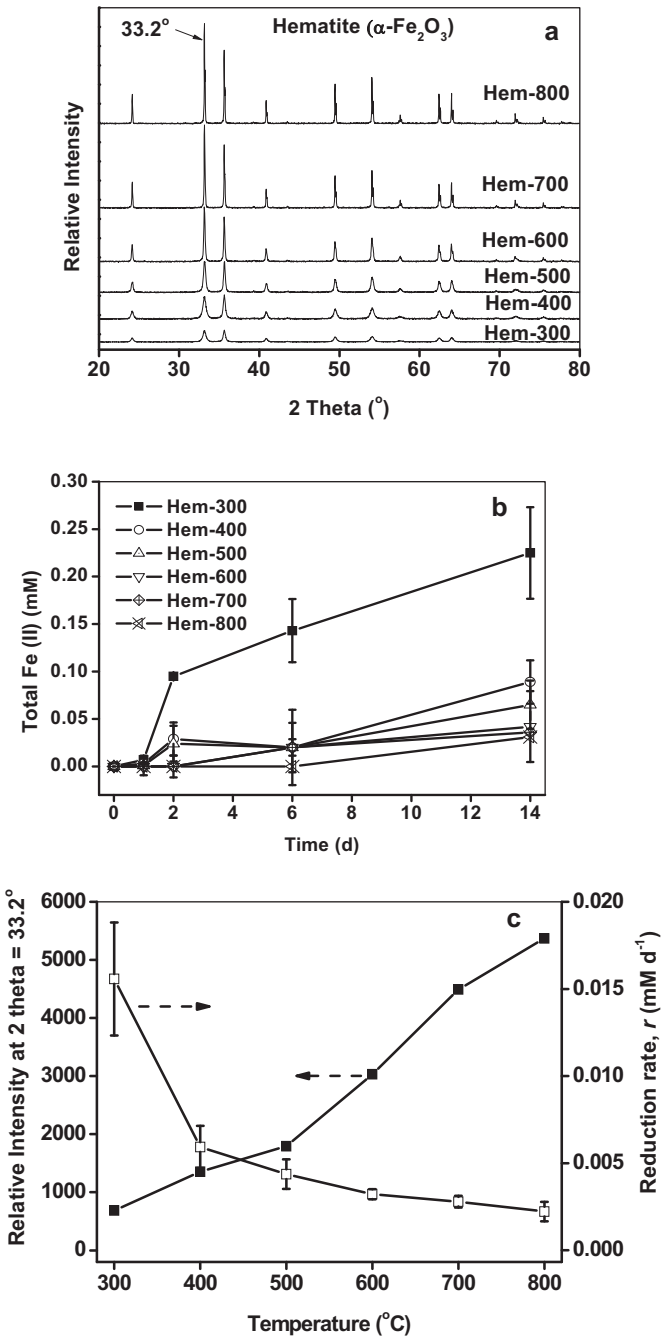

Fig. 2. (a) The XRD patterns of synthesized hematite (α-Fe_2O_3) at different temperatures (300–800 °C) for 2 h. (b) Total Fe(II) production during different hematite (α-Fe_2O_3) reductions by L17. (c) The comparison of peaks (1 0 1) and zero-order rate constants vs. calculation temperature. The initial concentrations of other substrates were all α-Fe_2O_3 (50 mM), L17 (1.5×10^8 cells mL^{-1}) and AQDS (100 μM). Data are means ± SD ($n = 3$).

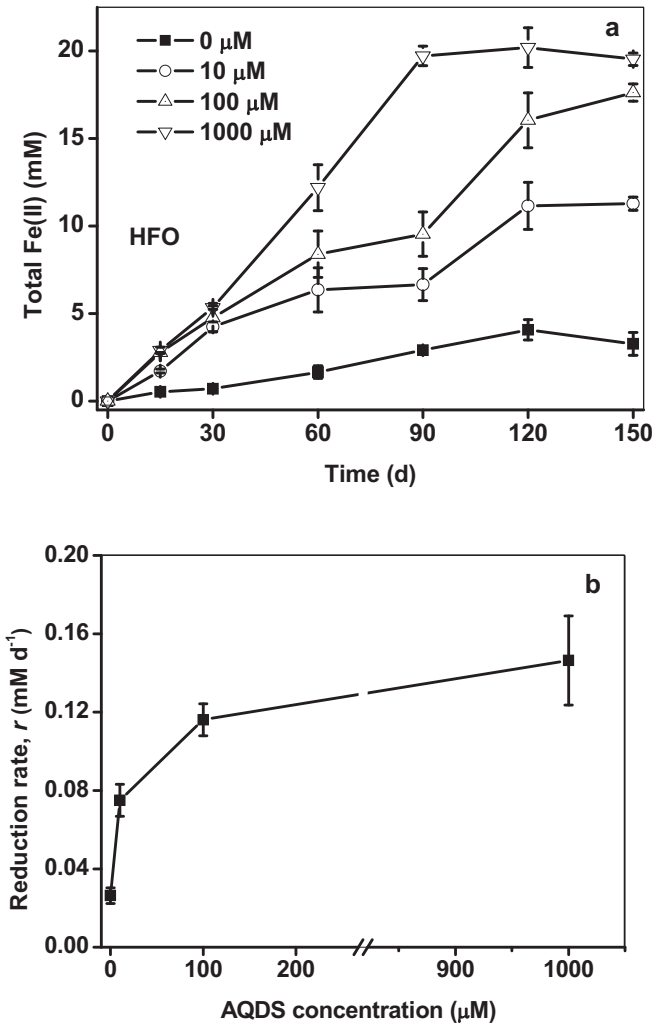

Fig. 3. Total Fe(II) production during HFO reduction by L17 with different concentrations of AQDS. The initial concentrations of other substrates were all HFO (50 mM), L17 (1.5×10^8 cells mL^{-1}) and AQDS (10 μM, 100 μM and 1000 μM). Data are means ± SD ($n = 3$).

3.4. Surface property changes during iron oxide reduction by L17

The surfaces of iron oxides changed after microbial reduction, which was first indicated by a visible change in the color of the reaction suspension (Fig. S1 in supporting information) that accompanied the production of Fe(II), especially in the inoculated vials with AQDS addition. They were dark red to brown for HFO, yellow to brown for α-FeOOH, orange to dark brown for γ-FeOOH and red to dark brown for α-Fe_2O_3, relative to the original color that remained in the sterile control vials throughout the experiment. To clearly illustrate the surface property changes during iron oxide reduction by L17, XRD and SEM–EDX were used to identify the structures and morphologies of the secondary minerals.

3.4.1. Crystal structure analyses

To characterize the crystal structure of iron oxides before and after microbial reduction by L17, the controls of four iron oxides and their two treatments (with L17 and with L17 + AQDS) were measured using XRD techniques [29]. Fig. 4 shows that the diffraction peaks of the four iron oxides were well matched with the JCPDS card but that the crystalline degree was considerably different. The peaks of α-FeOOH and α-Fe_2O_3 were very sharp, indicating the high crystalline degree of iron oxide, which was higher than that of γ-FeOOH and still showed good characteristic peaks. However, there were almost no diffraction peaks in the XRD patterns of HFO. In comparison with the two treatments, it was found that there were no significant changes in the XRD patterns in the presence of L17 alone, suggesting that the crystalline degree and structure was not obviously influenced by the addition of L17. However, when L17 and AQDS were added simultaneously, a new sharp peak appeared at $2\theta = 14^\circ$ for three types of iron oxides (HFO, α-FeOOH and γ-FeOOH). According to the JCPDS card, it may be the characteristic peak of $Fe_3(PO_4)_2 \cdot 8H_2O$ (vivianite), whereas another new peak at $2\theta = 32^\circ$ for HFO + L17 + AQDS may be the characteristic peak of $FeCO_3$ (siderite), but there was no new peak for the α-Fe_2O_3 even with L17 and AQDS. Since the iron-reducing capacity of L17 was weak but can be enhanced significantly in the presence of AQDS, the Fe(II) production of the former was much less than that of the latter with AQDS. Then, the generated Fe(II) can react with the phosphate and carbonate in the medium to form participations of $Fe_3(PO_4)_2 \cdot 8H_2O$ and $FeCO_3$. But the α-Fe_2O_3 was too stable to be reduced extensively because of its highest crystalline degree and stable crystal structure, resulting in no new phases appearing on the surface.

3.4.2. FTIR analysis

The reduction of these four types of iron oxides by L17 without/with AQDS was further examined by FTIR (Fig. 5). The broad peaks at 3000–3500 cm^{-1} and the strong peak at 1637 cm^{-1} are attributed to the O–H stretching vibration of water, Fe–OH group and hydrated species on the iron oxide surface. For HFO in Fig. 5a, compared with the HFO sample as a blank, some new peaks were found in the FTIR spectra of HFO + L17 and HFO + L17 + AQDS. For example, the peaks at 596 cm^{-1} and 1059 cm^{-1} were attributed to the vibration of Fe–O and P–O, respectively [30], whereas the peak intensity of HFO + L17 + AQDS was higher than that of HFO + L17. For α-FeOOH in Fig. 5b, the peaks of α-FeOOH + L17 and α-FeOOH + L17 + AQDS at 1062 cm^{-1} were attributed to the vibration of P–O. For γ-FeOOH in Fig. 5c, even though no new peak appeared in both γ-FeOOH + L17 and γ-FeOOH + L17 + AQDS, the intensity at 1000–1100 cm^{-1} increased clearly compared with γ-FeOOH, indicating some new peaks in this range, which may also be attributed to the vibration of P–O. For α-Fe_2O_3 in Fig. 5d, the weak peaks of α-Fe_2O_3 + L17 and α-Fe_2O_3 + L17 + AQDS at 1088 cm^{-1} were also attributed to the vibration of P–O. This result was well matched with the above XRD result, and it was further confirmed that the iron-reducing capacity of L17 can be enhanced significantly by AQDS.

3.4.3. Morphology and element analyses

Fig. 6 shows the SEM images of the four types of iron oxides before and after microbial iron reduction by L17. The results suggest that the morphologies of various iron oxides were different in that the HFO was a ruleless sheet structure, the α-FeOOH was an asymmetrically acicular structure, the γ-FeOOH was a thin sheet structure and the α-Fe_2O_3 was covered with fine particles. There were no significant changes in the morphology after the addition of L17, which was consistent with the results of iron reduction and XRD. This was because the capacity of iron oxide reduction by L17 was minor, and the dissolution and corrosion of iron oxides were too slight to change the surface morphology. When L17 and AQDS were added simultaneously, the iron reduction results showed a huge enhancement, and the XRD patterns also showed that some new phases such as $Fe_3(PO_4)_2 \cdot 8H_2O$ and $FeCO_3$ were generated on the surface but that the surface morphology did not change. This might be contributed to the fact that the amount of biogenic $Fe_3(PO_4)_2 \cdot 8H_2O$ and $FeCO_3$ were far away from that of the added iron oxides.

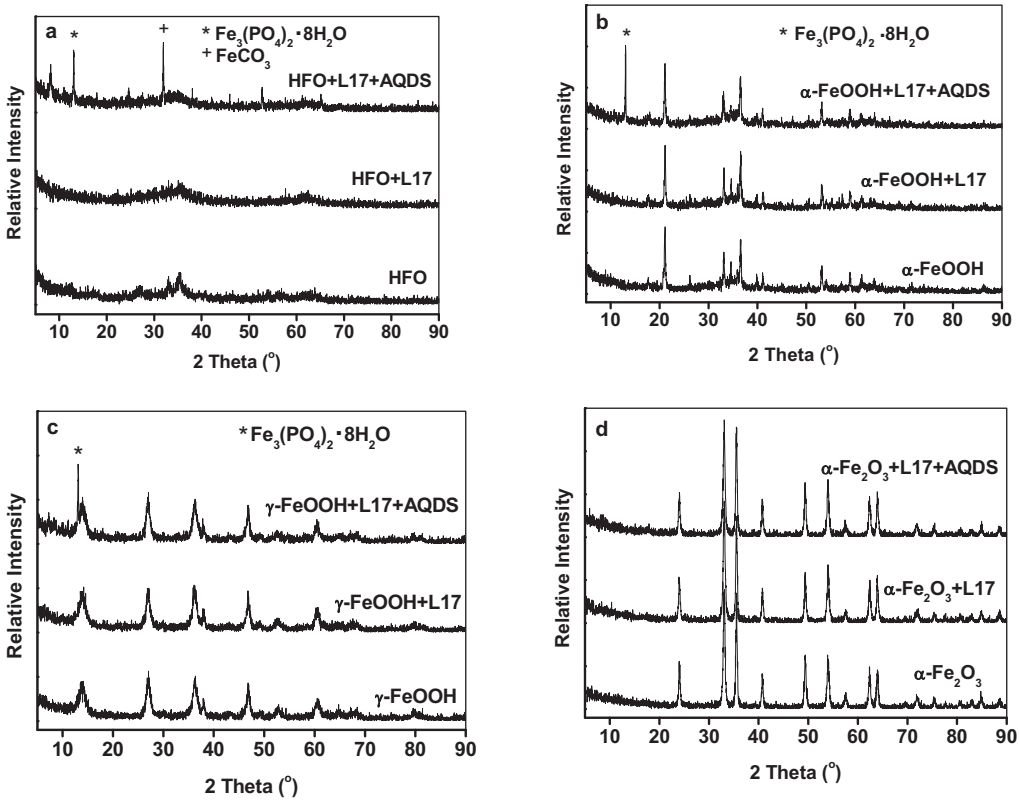

Fig. 4. XRD patterns of different Fe(III) oxides before and after microbial reduction by L17 with/without AQDS: (a) HFO, (b) α-FeOOH, (c) γ-FeOOH and (d) α-Fe_2O_3.

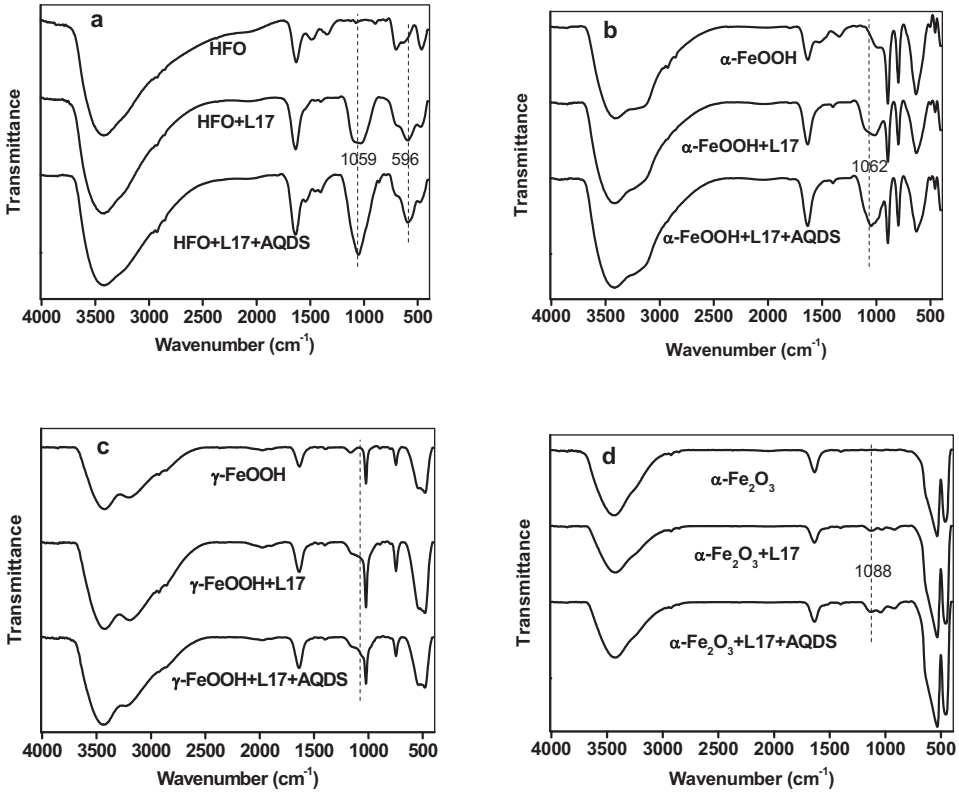

Fig. 5. FTIR spectra of different Fe(III) oxides before and after microbial reduction by L17 with/without AQDS: (a) HFO, (b) α-FeOOH, (c) γ-FeOOH and (d) α-Fe_2O_3.

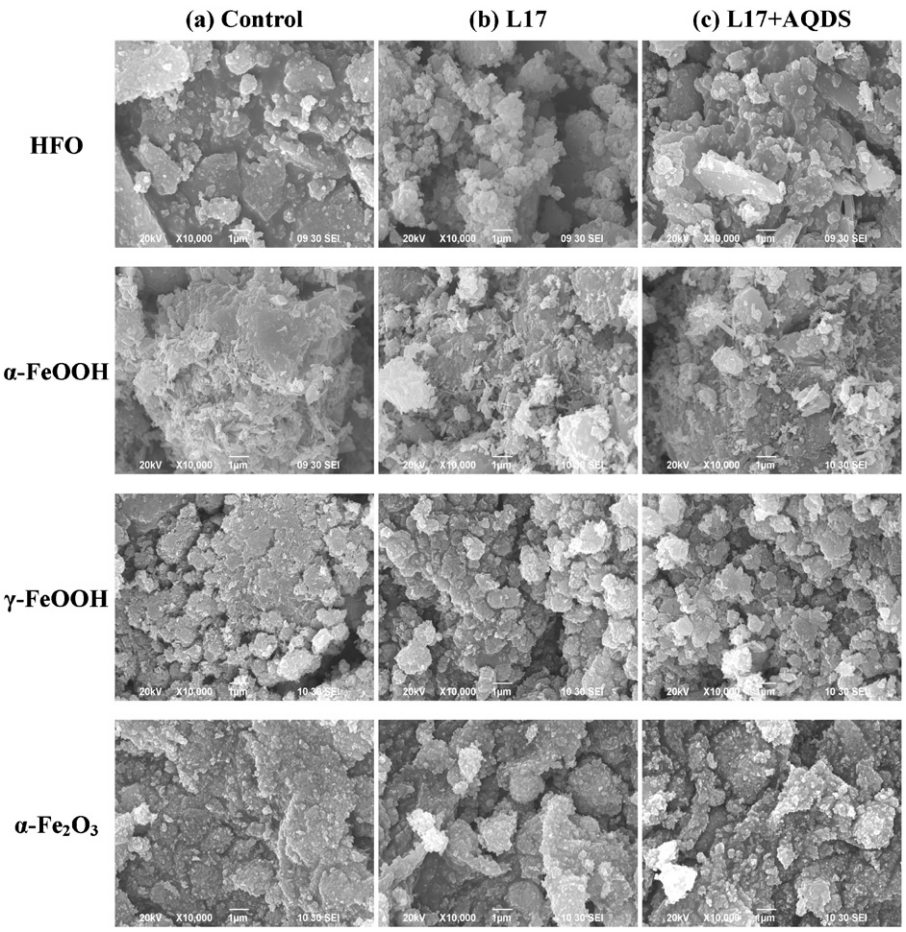

Fig. 6. SEM of iron oxides before and after microbial reductions by L17. (a) Four types of iron oxides (HFO, α-FeOOH, γ-FeOOH and α-Fe_2O_3). (b) Iron oxides with L17. (c) Iron oxides with both L17 and AQDS.

The element analyses by using EDX in Table 1 show the element dispersion of the four iron oxides before and after the addition of L17 and AQDS. It is noted that no phosphor was detected in the control, whereas the treatments with an addition of L17 and L17 + AQDS had phosphor on the surface, and the P amount with L17 + AQDS was higher than that of L17 alone. Based on these XRD results, biogenic Fe(II) can react with phosphate to form $Fe_3(PO_4)_2{\cdot}8H_2O$ precipitates. From the iron reduction results, the amount of biogenic Fe(II) in L17 with AQDS was higher than that in L17 alone, indicating that more $Fe_3(PO_4)_2{\cdot}8H_2O$ can be generated in L17 with AQDS and that the detection amount of phosphor in EDX results will be greater in such a system. This result further confirmed that the addition of AQDS clearly accelerated microbial iron reduction by L17.

Table 1
Distribution of elements on the surfaces of the four types of iron oxides (HFO, α-FeOOH, γ-FeOOH and α-Fe_2O_3) before and after reaction with L17.

	Fe	O	P
HFO	30.45	69.55	ND
HFO + L17	23.88	72.97	3.15
HFO + L17 + AQDS	16.09	80.59	3.31
α-FeOOH	21.48	78.51	ND
α-FeOOH + L17	25.22	73.49	1.30
α-FeOOH + L17 + AQDS	24.41	73.76	1.84
γ-FeOOH	18.47	81.52	ND
γ-FeOOH + L17	14.67	84.43	0.48
γ-FeOOH + L17 + AQDS	17.67	81.08	1.26
α-Fe_2O_3	22.23	77.78	ND
α-Fe_2O_3 + L17	15.86	83.71	0.05
α-Fe_2O_3 + L17 + AQDS	18.54	80.77	0.34

Previous research has found that the sorption and/or surface precipitation of Fe(II) to the surfaces of bacteria and Fe(III) minerals inhibit iron reduction [13]. In this study, the secondary minerals of $Fe_3(PO_4)_2{\cdot}8H_2O$ and $FeCO_3$ were covered on the surfaces of iron oxides; however, the inhibition was not observed for the first 25 days because the Fe(II) production amounts were much less than those of the total iron oxides, slightly influencing reduction rates. For the HFO reduction with 1000 μM AQDS, it can be noted that Fe(II) production was unchanged after 90 days, indicating the inhibition of the bioreduction, which may be because the secondary minerals of $Fe_3(PO_4)_2{\cdot}8H_2O$ and $FeCO_3$ accumulated and covered the surfaces to delay the reductive dissolution of iron oxides.

4. Conclusion

In this study, the microbial reduction of various iron oxides was measured in the absence and presence of AQDS, and the results of their iron reduction rates by L17 with/without AQDS vs. the surface areas of iron oxides suggested that the iron oxide reduction rate by L17 was obviously affected by the surface area but did not completely depend on it, especially for HFO. Increasing the crystalline degree of hematite decreased the rate of iron reduction, indicating that a higher crystalline degree inhibited the microbial iron reduction. The addition of AQDS significantly accelerated the microbial reduction of crystalline Fe(III) oxides, which may be because of the growth in cells and abiotic Fe(III) reduction by AH_2DS. Secondary minerals (e.g., vivianite ($Fe_3(PO_4)_2$) and siderite ($FeCO_3$)) were the biogenic Fe(II) solids formed upon the bioreduction of iron oxides.

Acknowledgements

The authors would thank the National Natural Science Foundations of China (no. 40901114) and "973" Program (no. 2010CB134508) for a financial support to this work.

Appendix A. Supplementary data

Supplementary data associated with this article can be found, in the online version, at doi:10.1016/j.colsurfa.2010.11.061.

References

[1] T. Borch, R. Kretzschmar, A. Kappler, P.V. Cappellen, M. Ginder-Vogel, A. Voegelin, A. Campbell, Biogeochemical redox processes and their impact on contaminant dynamics, Environ. Sci. Technol. 44 (2010) 15–23.
[2] T. Behrends, P. Van Cappellen, Transformation of hematite into magnetite during dissimilatory iron reduction—conditions and mechanisms, Geomicrobiol. J. 24 (2007) 403–416.
[3] S. Glasauer, P.G. Weidler, S. Langley, T.J. Beveridge, Controls on Fe reduction and mineral formation by a subsurface bacterium, Geochim. Cosmochim. Acta 67 (2003) 1277–1288.
[4] D.P. Jaisi, H. Dong, C. Liu, Kinetic analysis of microbial reduction of Fe(III) in nontronite, Environ. Sci. Technol. 41 (2007) 2437–2444.
[5] J.K. Fredrickson, Y.A. Gorby, Environmental processes mediated by iron-reducing bacteria, Curr. Opin. Biotechnol. 7 (1996) 287–294.
[6] D.J. Scala, E.L. Hacherl, R. Cowan, L.Y. Young, D.S. Kosson, Characterization of Fe(III)-reducing enrichment cultures and isolation of Fe(III)-reducing bacteria, Res. Microbiol. 157 (2006) 772–783.
[7] D.R. Lovley, D.E. Holmes, K.P. Nevin, Dissimilatory Fe(III) and Mn(IV) reduction, Adv. Microb. Physiol. 49 (2004) 219–286.
[8] D.R. Lovley, E.J.P. Phillips, Novel mode of microbial energy metabolism: organic carbon oxidation coupled to dissimilatory reduction of iron or manganese, Appl. Environ. Microbiol. 54 (1988) 1472–1480.
[9] E.E. Roden, Geochemical and microbiological controls on dissimilatory iron reduction, C. R. Geosci. 338 (2006) 456–467.
[10] D.R. Lovley, Dissimilatory Fe(III) and Mn(IV) reduction, Microbiol. Rev. 55 (1991) 259–287.
[11] S. Bonneville, P.V. Cappellen, T. Behrends, Microbial reduction of iron(III) oxyhydroxides—effects of mineral solubility and availability, Chem. Geol. 212 (2004) 255–268.
[12] E.E. Roden, J.M. Zachara, Microbial reduction of crystalline iron(III) oxides influence of oxide surface area and potential for cell growth, Environ. Sci. Technol. 30 (1996) 1618–1628.
[13] R.A. Royer, B.A. Dempsey, B.H. Jeon, W.D. Burgos, Inhibition of biological reductive dissolution of hematite by ferrous iron, Environ. Sci. Technol. 38 (2004) 187–193.
[14] C. Liu, J.M. Zachara, N.S. Foster, J. Strickland, Kinetics of reductive dissolution of hematite by bioreduced anthraqinone-2,6-disulfonate, Environ. Sci. Technol. 41 (2007) 7730–7735.
[15] J. Jiang, A. Kappler, Kinetics of microbial and chemical reduction of humic substances: implications for electron shuttling, Environ. Sci. Technol. 42 (2008) 3563–3569.
[16] E.J. O'Loughlin, Effects of electron transfer mediators on the bioreduction of lepidocrocite (γ-FeOOH) by *Shewanella putrefaciens* CN32, Environ. Sci. Technol. 42 (2008) 6876–6882.
[17] M. Wolf, A. Kappler, J. Jiang, R.U. Meckenstock, Effects of humic substances and quinones at low concentrations on ferrihydrite reduction by *Geobacter metallireducens*, Environ. Sci. Technol. 43 (2009) 5679–5685.
[18] E.J. O'Loughlin, P. Larese-Casanova, S. Michelle, R. Cook, Green rust formation from the bioreduction of γ-FeOOH (lepidocrocite): comparison of several *Shewanella* species, Geomicrobiol. J. 24 (2007) 211–230.
[19] B.Z. Yan, B.A. Wrenn, S. Basak, P. Biswas, D.E. Giammar, Microbial reduction of Fe(III) in hematite nanoparticles by *Geobacter sulfurreducens*, Environ. Sci. Technol. 42 (2008) 6526–6531.
[20] X.M. Li, S.G. Zhou, F.B. Li, C.Y. Wu, L. Zhuang, W. Xu, L. Liu, Fe(III) oxide reduction and carbon tetrachloride dechlorination by a newly isolated *Klebsiella pneumoniae* strain L17, J. Appl. Microbiol. 106 (2009) 130–139.
[21] M.L. McCormick, P. Adriaens, Carbon tetrachloride transformation on the surface of nanoscale biogenic magnetite particles, Environ. Sci. Technol. 38 (2004) 1045–1053.
[22] U. Schwertmann, R.M. Cornell, Iron Oxides in the Laboratory: Preparation and Characterization, VCH, New York, 1991.
[23] F.B. Li, X.Z. Li, X.M. Li, T.X. Liu, J. Dong, Heterogeneous photodegradation of bisphenol A with iron oxides and oxalate in aqueous solution, J. Colloid Interface Sci. 311 (2007) 481–490.
[24] F.W. Picardal, R.G. Arnold, B.B. Huey, Effects of electron donor and acceptor conditions on reductive dehalogenation of tetrachloromethane by *Shewanella putrefaciens* 200, Appl. Environ. Microbiol. 61 (1995) 8–12.
[25] K.L. Straub, M. Benz, B. Schink, Iron metabolism in anoxic environments at near neutral pH, FEMS Microbiol. Ecol. 34 (2001) 181–186.
[26] C. Liu, S. Kota, J.M. Zachara, J.K. Fredrickson, C.K. Brinkman, Kinetic analysis of the bacterial reduction of goethite, Environ. Sci. Technol. 35 (2001) 2482–2490.
[27] E.E. Roden, Fe(III) oxide reactivity toward biological versus chemical reduction, Environ. Sci. Technol. 37 (2003) 1319–1324.
[28] D.R. Lovley, J.D. Coates, E.L. Blunt-Harris, E.J.P. Phillips, J.C. Woodward, Humic substances as electron acceptors for microbial respiration, Nature 382 (1996) 445–448.
[29] J.G. Yu, Q.J. Xiang, M.H. Zhou, Preparation, characterization and visible-light-driven photocatalytic activity of Fe-doped titania nanorods and first-principles study for electronic structures, Appl. Catal. B 90 (2009) 595–602.
[30] L. Legrand, L. Mazerolles, A. Chaussé, The oxidation of carbonate green rust into ferric phases: solid-state reaction or transformation via solution, Geochim. Cosmochim. Acta 68 (2004) 3497–3507.